Scaling of the flowfield in a combustion chamber with a gas–gas injector*

Wang Xiao-Wei(汪小卫)†, Cai Guo-Biao(蔡国飙), and Jin Ping(金 平)

School of Astronautics, Beijing University of Aeronautics and Astronautics, Beijing 100191, *China*

(Received 18 April 2009; revised manuscript received 5 June 2009)

The scaling of the flowfield in a gas–gas combustion chamber is investigated theoretically, numerically and experimentally. To obtain the scaling criterion of the gas–gas combustion flowfield, formulation analysis of the three-dimensional (3D) Navier–Stokes equations for a gaseous multi-component mixing reaction flow is conducted and dimensional analysis on the gas–gas combustion phenomena is also carried out. The criterion implies that the size and the pressure of the gas–gas combustion chamber can be changed. Based on the criterion, multi-element injector chambers with different geometric sizes and at different chamber pressures ranging from 3 MPa to 20 MPa are numerically simulated. A multi-element injector chamber is designed and hot-fire tested at five chamber pressures from 1.64 MPa to 3.68 MPa. Wall temperature measurements are used to understand the similarity of combustion flowfields in the tests. The results have verified the similarities between combustion flowfields under different chamber pressures and geometries, with the criterion applied.

Keywords: scaling, similarity, gas–gas combustion, experiment
PACC: 9480, 9530L, 5275D, 4790

1. Introduction

Scaling of combustion devices for liquid propellant rocket engines (LPREs) has been a subject of considerable difficulty and controversy since the advent of rocketry. Nevertheless, the use of scaling techniques is invaluable. The cost and the cycle can be sharply reduced by using subscale devices at lower pressure (model) to develop full-scale ones (prototype).[1−5] The first formal liquid rocket scaling research was conducted by Penner more than 50 years ago,[1,2] but the studies have made no progress since then, owing to some historical reasons. However, in the current era it has been picked up by designers because of the higher requirements for performance and significant reduction in financing.[3−5]

The full flow stage combustion (FFSC) cycle engine is preferable because of its high performance and high reliability.[6] Gas–gas combustion technology is a key technology for this kind of engine. Although a lot of studies have been carried out until now,[7−19] the scaling of gas–gas combustion is, unfortunately, not involved. The FFSC nominal gas–gas injector main thrust chamber was designed at a chamber pressure of above 20 MPa and mass flowrate of above 450 kg/s. Also, gas–gas injectors have been widely used on other engines and combustion devices.[19,20] Thus it will be very valuable if a feasible scaling technique can be applied to the development of gas–gas injector chambers.

The scaling technique of liquid rocket engine combustion devices was investigated and reviewed in Refs. [3]–[5], where it was stated that because almost all major design requirements for combustion devices, including performance, stability, and compatibility, originate from the injector, scaling is significantly dependent on injection processes, and further concluded that the combustion process is the source for understanding how to scale performance, stability, and compatibility in liquid rocket combustion chambers. Additionally, the key issue of the scaling technique is to ensure similarity of the phenomena between the model and prototype. Therefore, the key issue of ensuring similarity of the phenomena in the chambers is to ensure the similarity of the combustion flowfields.

The spray combustion process is composed of injection, atomization, vaporization, mixing and reaction. Because of its complexity and the strongly coupled relationships between them, scaling of the spray reacting flows with complete similarity is found to be impossible in practice. Thus, scaling of combustion devices for LPREs has not been fully developed yet,

*Project supported by the National High Technology Research and Development Program of China (Grant No. 2007AA7023) and the Innovation Foundation of BUAA for Ph.D Graduates (Grant No. 430569).
†Corresponding author. E-mail: wangxwbuaa@163.com
© 2010 Chinese Physical Society and IOP Publishing Ltd

and James R. Hulka also concluded that an LPRE combustor-based research programme that evaluates the rationale and effectiveness of scaling was probably not affordable in the foreseeable future and a significant research-oriented evaluation of scaling of LPRE combustion devices would eventually require the evaluation of all the individual processes as well as their interactions. Nevertheless, the gas–gas combustion process only involves injection, mixing and reaction. The characteristics of the gas–gas injector chamber indicate a possibility of guaranteeing the similarity in whole between model and prototype. In the present paper the necessary and the sufficient conditions for the scaling of the gas–gas combustion flowfield are studied theoretically, numerically and experimentally.

In the present paper, to obtain the scaling criterion of the gas–gas combustion flowfield, a formulation analysis of the 3D Navier–Stokes equations for gaseous multi-component mixing reaction flow is conducted, and a dimensional analysis and the π theorem are also applied to the analysis on the gas–gas combustion phenomena. Based on the criterion, multi-element injector chambers of different geometric sizes and at different chamber pressures ranging from 3 MPa to 20 MPa are numerically simulated, and corresponding hot-fire test experiments are carried out at five different pressures ranging from 1.5 to 3.68 MPa by utilizing a multi-element injector chamber equipped with seven shear-coaxial elements.

2. Fomulation analysis

2.1. The Navier–Stokes equations

In gas–gas mixing combustion phenomena, gaseous oxidizers and gaseous fuels are injected into the combustors through their respective passages, and then mix and combust with each other. The Mach number M of the flows in the combustion devices of LPREs or other types of engine is commonly lower than 1.0, and when the flows are in a steady state, the non-dimensional 3D equations governing gaseous multi-component combustion flow are given as follows:[21]

$$\frac{\partial}{\partial x_{j*}}\left(\rho * u_{j*}\right) = 0, \tag{1}$$

$$\frac{\partial}{\partial x_j^*}(\rho^* u_i^* u_j^*) = \left(\frac{1}{\mathrm{Fr}^2}\right)\rho^* F^* - (\mathrm{Eu})\frac{\partial p^*}{\partial x_i^*} + \left(\frac{1}{\mathrm{Re}}\right)\frac{\partial}{\partial x_j^*}\left[\mu^*\left(\frac{\partial u_i^*}{\partial x_j^*} + \frac{\partial u_j^*}{\partial x_i^*}\right)\right] + \left(\frac{\lambda_0}{\mu_0}\frac{1}{\mathrm{Re}}\right)\frac{\partial}{\partial x_i^*}\left[\lambda^*\frac{\partial u_j^*}{\partial x_j^*}\right], \tag{2}$$

$$\frac{\partial}{\partial x_j^*}\left(\rho^* u_j^* Y_i^*\right) = \left(\frac{1}{\mathrm{ScRe}}\right)\frac{\partial}{\partial x_j^*}\left(\mu^*\frac{\partial Y_i^*}{\partial x_j^*}\right) - \frac{w_{\mathrm{s}\infty}}{\rho_\infty U_\infty / L} w_{\mathrm{s}}^*, \tag{3}$$

$$c_{\mathrm{p}}^*\frac{\partial}{\partial x_j^*}(\rho^* u_j^* T^*) = \left(\frac{1}{\mathrm{RePr}}\right)\frac{\partial}{\partial x_j^*}\left(\mu^* c_{\mathrm{p}}^*\frac{\partial T^*}{\partial x_j^*}\right) + w_{\mathrm{s}}^* Q_{\mathrm{s}}^*\frac{\mathrm{Da}_2}{\mathrm{Pe}}, \tag{4}$$

where $\mathrm{Fr} = \dfrac{U_\infty}{\sqrt{gL}}$, $\mathrm{Eu} = \dfrac{p_\infty}{\rho_\infty U_\infty^2}$, $\mathrm{Re} = \dfrac{\rho_\infty U_\infty L}{\mu_\infty}$, $\mathrm{Sc} = \dfrac{\mu}{\rho D}$, $\mathrm{Pr} = \dfrac{\mu c_{\mathrm{p}}}{\lambda}$, $\mathrm{Pe} = \mathrm{RePr}$, and $\mathrm{Da}_2 = \dfrac{w_{\mathrm{s}\infty} Q_{\mathrm{s}}}{\lambda_\infty T_\infty / L^2}$.

Constancy of all dimensionless groups for all processes between different combustion chambers ensures that the processes are strictly similar; they are summarized as follows: Fr_1=Fr_2, Eu_1=Eu_2, Re_1=Re_2, Sc_1=Sc_2, Pr_1=Pr_2, and Da_{21}=Da_{22}.

2.2. Monodromy condition analysis

The similarity theory indicates that similarity between phenomena of the same type still requires that between their monodromy conditions. Here the conditions are given as follows:

1) Geometric condition: geometric similarity.

2) Inlet conditions:

a) The velocity distributions of propellants at inlets: $u_1 = u_2 = \mathrm{idem}$,

b) The temperature distributions of propellants at inlets: $T_1 = T_2 = \mathrm{idem}$,

c) The species concentration distributions at inlets: $Y_1 = Y_2 = \mathrm{idem}$.

3) Wall boundary conditions:

a) Velocity boundary conditions: non-slip condition: $\partial v/\partial n = 0$,

b) Heat boundary condition: $\dot{q} = 0$ or $Nu_1 =$

Nu_1,

c) Wall species boundary conditions: non existence or similar wall species boundary conditions.

4) Outlet condition: limiting conditions are not necessary due to the supersonic flow in the nozzle.

2.3. Similarity criterion analysis

As the similarity theory indicates, to assure that the phenomena are strictly similar, the whole of the criteria should be satisfied, but in fact it is always impossible to meet the whole of the criteria. The similarity theory also indicates that each similarity criterion plays a role with its own importance. Some subordinate criteria that have little influence on the phenomenon can be ignored through analysing each criterion itself.[22] The analysis of the nondimensional groups and the monodromy conditions are given as follows:

1) Fr

Fr $= U_\infty/\sqrt{gL}$ is the ratio of inertial force to gravitational force, indicating the influence of the gravitational force. It can be ignored in the ground testing of a rocket.[22]

2) Eu

Eu indicates the effects of surface forces. It is always important for studying the phenomena of water hammer and cavitation. In this study it is not a main factor.[22] Additionally,

$$\mathrm{Eu} = \frac{p_\infty}{\rho_\infty U_\infty^2} = \frac{R_\infty T_\infty}{U_\infty^2},$$

it is very easy to ensure that $R_\infty T_\infty$ is constant, thus ensuring that Eu is constant as long as the characteristic velocity is unchanged.

3) Re

Re is the ratio of inertial force to viscous force in the unit volume. The density of the gaseous propellant is almost proportional to the pressure, while pressure hardly influences the viscosity of the gaseous propellant. When characteristic velocity u is kept unchanged, to ensure that Re is constant, the characteristic dimension must be inversely proportional to the pressure, leading to an impractically large size of the model at low pressures. However, there exists what is called the 'self-similar zone' of liquid flows. When Re exceeds a specific value, the flow is in a sufficiently turbulence condition and enters the 'second self-similar zone', such as jet flow, mixing layer flow, boundary layer flow and pipe flow. Thus when the flows of model and prototype are in the 'self-similar zone', they are similar as long as the monodromy conditions are similar.[22]

In the gas–gas injector chamber, the Re of the gaseous propellant jets is always very high. The gas–gas combustion flowfield always stays in sufficient turbulence conditions. The flows have entered the 'second self-similar zone'. The values of Re of model and prototype are not required to be the same.

4) Pr, Sc

These belong to the basic property parameters and must be ensured to be constant. When identical gaseous propellants are used, Pr and Sc are kept constant.

5) Da_2

Da_2 is to evaluate the influence degree of the reaction rate and diffusion on the flow. In a rocket engine combustor at high temperature and high pressure, the $\mathrm{H}_2/\mathrm{O}_2$ reaction always occurs very fast, especially when the reactants are in the gaseous state.[21] The gas–gas combustion process differs from the spray combustion process in that the atomization and vaporization are not present. In the gas–gas combustion chamber, the diffusion mainly controls the flow, the gases reaction process is completed in a much shorter time than the diffusion and convection processes in the combustor, and the reaction time can be ignored compared with diffusion time and convection time.[12,15,16,18] Therefore, in the gas–gas combustion chamber, the influence of the reaction on the flow can be ignored and Da_2 is a subordinate one.

6) The inlet conditions

At the inlet of the mixing zone, namely the outlets of the injectors, the mean velocities of the propellant jets can be easily kept constant by changing the propellant mass flowrate proportional to the chamber pressure and the injection area. However, keeping the velocity profiles rigorously consistent is sometimes hard, which requires that the whole hardware inlet conditions of the model and the prototype are similar, while the jets are always in a sufficiently turbulence state, and according to the self-similar character of turbulence flow, the distribution of velocities must be constant when the mean velocities are unchanged. Even though there exist some differences in distribution, they can also be disregarded as long as they have no notable effect on the flow.

The analysis above can also be applied to the temperature distribution inlet condition. Also, the species concentration distribution inlet condition can be ensured easily by offering identical propellants.

7) Wall boundary conditions

Generally, the wall non-slip and similar species boundary conditions can be covered naturally in a regeneratively-cooled chamber. The wall species boundary conditions are assumed to be similar if there exist any conditions of this kind. Greater or lower heat flux from the productions to the chamber wall occurs. The heat wall boundary condition requires Nu_1=Nu_2. Nu implies the non-dimensional temperature gradient of the flow near the wall, and it is important for studying the wall heat transfer. However, the object of this study is the similarity of the whole flow, and the heat transfer through the chamber wall hardly influences the whole flow in non-micro or non-small engines, except for the flow in the near-wall zone. Therefore, as another subordinate factor, the influence of heat loss from the combustor walls can also be neglected.

Based on the analyses above, according to the similarity theorem, the necessary and sufficient conditions of similarity of the combustion flowfield in the gas–gas combustion chamber are concluded as follows: a) similarity between the geometries of the injector and chamber; b) identical propellants; c) constant injection velocities and propellant temperatures; d) non-slip and similar species wall boundary.

3. Dimensional analysis

Dimensional analysis is another theoretical method which can effectively serve the experimental studies. This method has wider applicability;[23] unfortunately, its application to the phenomena in LPREs has not yet been found. In this section, dimensional analysis is applied to the gas–gas combustion phenomena to obtain the scaling criterion and give a further understanding of the gas–gas combustion process, and also provide a reference for other flows in LPREs or other combustion devices.

Without loss of generality, the shear-coaxial injector widely applied in H_2/O_2 LPREs is used as an illustrative example. Gaseous oxygen and gaseous hydrogen are chosen as the propellants. The same analysis can be utilized in other kinds of LPREs or combustion devices. The parameters related to the gas–gas combustion process in LPREs are length L, speed u, pressure P, temperature T, species concentration Y, density ρ, viscosity μ, specific heat $C_{\rm p}$, diffusivity D, heat conduction λ, the wall species boundary parameter G, heat flux loss $\dot{q}$, reaction rates $w_{\rm s}$, and reaction heat $Q_{\rm s}$. The specific monodromy conditions determine the unique solutions of the same kind of physical phenomena. The specific independent parameters related to the shear-coaxial gas–gas injector mixing process are summarized in Table 1.

Table 1. Independent parameters related to the shear-coaxial gas–gas injector mixing flowfield.

geometric parameters	injector characteristic geometries: central O_2 post inner diameter d_{O_2}, annular passage inner diameter $d_{H_{21}}$, annular passage outer diameter $d_{H_{22}}$, recess length or other characteristic size $L_{\rm r}$;
	Chamber characteristic geometry: inner combustor diameter $d_{\rm c}$;
velocity parameters	injection velocities: u_{H_2}, u_{O_2}
pressure parameter	back pressure $p_{\rm c}$
property parameters	ρ_{H_2} ρ_{O_2}, μ_{O_2}, μ_{H_2}, Cp_{H_2}, Cp_{O_2}, T_{H_2}, T_{O_2}, λ_{H_2}, λ_{O_2}, Y_{H_2}, Y_{O_2}, D_{H_2}, D_{O_2}
wall boundary parameters in combustor	heat flux loss $\dot{q}$, species boundary parameter G, non-slip condition
reaction parameters	$w_{\rm si}$ (i=H_2, O_2, H_2O, ...), $Q_{\rm s}$

3.1. π Theorem

In tests of gas–gas injectors, the combustion length $L_{\rm com}$ is always used to evaluate the performance of the mixing combustion process.[10,18,19] A specific $L_{\rm com}$ represents a specific flowfield structure in gas–gas combustion flow. In the study, $L_{\rm com}$ is chosen as the research object, and an expression for $L_{\rm com}$ will be obtained by using the π theorem.

First of all, the parameters that can influence $L_{\rm com}$ should be found. Each parameter in Table 1 may have more or less influence on $L_{\rm com}$. Previous studies indicated that the propellant temperature could influence the whole combustion flow.[19] Therefore, as a precondition, here the propellants and their temperatures are assumed to be unchanged, then some relevant parameters (μ_{O_2}, μ_{H_2}, Cp_{H_2}, Cp_{O_2}, T_{H_2}, T_{O_2}, λ_{H_2}, λ_{O_2}, Y_{H_2}, Y_{O_2}, D_{H_2}, D_{O_2} $Q_{\rm s}$) are constant. In general, the wall species boundary condi-

tion in a common chamber does not exist, especially in the regeneratively-cooled chamber. Even if some wall species boundaries exist, the wall species boundary conditions for model and prototype are assumed to be similar here.

Therefore, the parameters that still influence $L_{\rm com}$ are $d_{\rm O_2}$, $d_{\rm H_{21}}$, $d_{\rm H_{22}}$, $L_{\rm r}$, $d_{\rm c}$, $u_{\rm H_2}$, $u_{\rm O_2}$, $\rho_{\rm H_2}$, $\rho_{\rm O_2}$, $p_{\rm c}$, $\dot{q}$, and $w_{\rm si}$. The expression of $L_{\rm com}$ can be obtained as follows

$$L_{\rm com} = f(d_{\rm O_2}, d_{\rm H_{21}}, d_{\rm H_{22}}, {\rm Lr}, d_{\rm c}, u_{\rm O_2}, u_{\rm H_2}, \rho_{\rm O_2}, \rho_{\rm H_2}, p_{\rm c}, \dot{q}, w_{\rm si}). \quad (5)$$

The basic units contained in these parameters are L (length), T (time), M (mass), and $d_{\rm O_2}$, $u_{\rm O_2}$, $\rho_{\rm O_2}$ are chosen as the basic parameters. As a result, for the application of the π theorem, ten dimensionless parameters are introduced as follows:

$$\pi_1 = \frac{L_{\rm com}}{d_{\rm O_2}}, \quad \pi_2 = \frac{d_{\rm H_{21}}}{d_{\rm O_2}}, \quad \pi_3 = \frac{d_{\rm H_{22}}}{d_{\rm O_2}},$$

$$\pi_4 = \frac{L_{\rm r}}{d_{\rm O_2}}, \quad \pi_5 = \frac{d_{\rm c}}{d_{\rm O_2}}, \quad \pi_6 = \frac{\rho_{\rm O_2}}{\rho_{\rm H_2}},$$

$$\pi_7 = \frac{p_C}{\rho_{\rm O_2} \cdot u_{\rm O_2}^2}, \quad \pi_8 = \frac{u_{\rm H_2}}{u_{\rm O_2}}, \quad \pi_9 = \frac{\dot{q}}{\rho_{\rm O_2} \cdot u_{\rm O_2}^3},$$

and

$$\pi_{10} = \frac{w_{si}}{\rho_{\rm O_2} \cdot u_{\rm O_2}/d_{\rm O_2}}.$$

Thus the following expression can be obtained: $\pi_1 = f(\pi_2, \ldots, \pi_{10})$.

Because of convenient analysis here, the dimensional analysis can be conducted under a precondition mentioned above. Thus, the educed dimensionless parameters are not the same as those obtained in Subsection 2.1 on formulation analysis.

3.2. Similarity criterion analysis

Equation 2 indicates that π_1 is unchanged as long as $\pi_2, \ldots, \pi_{10}$ are kept constant, and

$\pi_2 = d_{\rm H_{21}}/d_{\rm O_2}$ is the ratio of annular passage inner diameter to O_2 post inner diameter, implying the influence of the O_2 post tip thickness on the combustion flow;

$\pi_3 = d_{\rm H_{22}}/d_{\rm O_2}$ is the ratio of annular passage outer diameter to O_2 post inner diameter, implying the influence of injection area ratio on the combustion flow.

$\pi_4 = L_{\rm r}/d_{\rm O_2}$ indicates the influence on the combustion flow of the recess length or other characteristic size of the injector.

$\pi_5 = d_{\rm c}/d_{\rm O_2}$ is the ratio of chamber inner diameter to O_2 post inner diameter, and indicates the influence of the chamber geometry on the combustion flow.

$\pi_6 = \rho_{\rm O_2}/\rho_{\rm H_2}$ indicates the influence of the density ratio of oxidizer to fuel on the combustion flow.

$\pi_7 = p_{\rm c}/(\rho_{\rm O_2} \cdot u_{\rm O_2}^2) = 1/(R_{\rm O_2} T_{\rm O_2} \cdot u_{\rm O_2}^2)$ is the ratio of chamber pressure to O_2 injection dynamic pressure, implying the influence of O_2 injection velocity on the combustion flow.

$\pi_8 = u_{\rm H_2}/u_{\rm O_2}$ indicates the influence of injection velocity ratio on the combustion flow.

$\pi_9 = \dot{q}/(\rho_{\rm O_2} \cdot u_{\rm O_2}^3)$ is the ratio of heat loss rate to characteristic dynamic heat flux rate, showing the influence of heat loss rate on the combustion flow.

$\pi_{10} = w_{\rm si}/(\rho_{\rm O_2} \cdot u_{\rm O_2}/d_{\rm O_2})$ indicates the contrast in degrees between the effects of the chemical reaction dynamic rate and the convection removal rate on the combustion flow. Firstly, keeping the geometric similarities of the injectors and combustors can ensure that parameters $\pi_2 - \pi_5$ are constant and

$$\pi_6 = \frac{\rho_{\rm O_2}}{\rho_{\rm H_2}} = \frac{\dfrac{p_{\rm c}}{R_{\rm O_2} T_{\rm O_2}}}{\dfrac{p_{\rm c}}{R_{\rm H_2} T_{\rm H_2}}} = \frac{R_{\rm H_2} T_{\rm H_2}}{R_{\rm O_2} T_{\rm O_2}} = \text{const.} \quad (6)$$

Due to the compressibility of gaseous propellants, π_7 and π_8 can be kept constant as long as the injection pressure drop ratios are kept constant.

π_{10} implies the influence degree of the chemical reaction rate and the convection removal rate on the mixing combustion process. In the above section, the analysis of Da_2 indicates that in a rocket engine combustor at high temperature and high pressure, the H_2/O_2 reaction always occurs very fast, especially when the reactants are in the gaseous state. In a gas–gas combustion chamber with a high Re, the diffusion and the convection mainly control the flow; the gases' chemical reaction process is completed in a much shorter time than the diffusion and convection processes in the combustor, and the reaction time can be ignored compared with the diffusion time and the convection time. Therefore, according to the similarity theory, π_{10} as a subordinate factor can be ignored in this analysis.

The analysis of π_9 which represents the influence on the flowfield of the heat loss that always occurs on the chamber walls is given as follows.

1) Constant chamber pressure

When the chamber pressure is kept constant, the $\rho_{\rm O_2}$ will be constant. Thus, as long as the O_2 injection velocity is unchanged, according to the heat transfer

theory of LPREs, the heat flux $\dot{q}$ will be constant, which results in the fact that π_9 does not vary.

2) Varying chamber pressures

According to the heat transfer theory of LPREs, $\dot{q}$ is proportional to 0.8 power of chamber pressure: $\dot{q} \sim p^{0.8}$, and when u_{O_2} is unchanged, π_9 will be inversely proportional to 0.2 power of chamber pressure, which shows that the chamber pressure does not intensely influence π_9. Additionally, the object of this study is the similarity of the whole flow, and the heat transfer through the chamber wall hardly influences the whole flow in non-micro or non-small engines except for the near-wall zone. Therefore, as a subordinate factor, the influence of heat loss from the combustor walls can also be neglected.

Based on the preconditions mentioned in Subsection 3.1 and the analysis in Subsection 3.2, the criterion for keeping π_1 constant is summarized as follows: a) geometric similarities of the injector and chamber; b) identical propellants; c) constant injection velocity and propellant temperature; d) non-slip wall boundary and similar wall species boundary. This criterion ensures the constancy of π_1, namely it ensures that the gas–gas combustion flowfields are similar. It is the same as the results of the formulation analysis in the last section.

The scaling criterion of the combustion flowfield obtained above solves the key problem of the performance and heat transfer scaling technologies of gas–gas combustion devices. In the scaling method in this study, photo-scaled injector elements are adopted. This method was first suggested by Hewitt[24] based on empirical combustion stability data,[24] and later it was developed into many forms, including the most recent one.[25]

The scaling criterion indicates that the combustion flowfields can be similar when the geometries are similar and the chamber pressure is variable. Therefore, a small-size model engine at low pressures and in small flowrate conditions can be designed to simulate the prototype engine as long as the scaling criterion is satisfied.

4. Numerical study

Model and prototype multi-element gas–gas injector chambers were designed, and gaseous oxygen and gaseous hydrogen were chosen as the propellants. The shear-coaxial injector which has been widely applied in H_2/O_2 LPREs was used. According to the criterion, the combustion flowfields were calculated in two steps for clearer understanding. First, chamber pressure was kept constant, and the prototype and model chambers had different sizes. Second, the sizes were kept constant, and the chambers were designed at different pressures. The propellant flowrates changed in both steps.

The chamber parameters were chosen from the operating range of real engines. The characteristic lengths of the two chambers are both 935 mm, and their compression ratios are 3.7. The prototype injector element structure and the chamber are shown in Fig. 1.

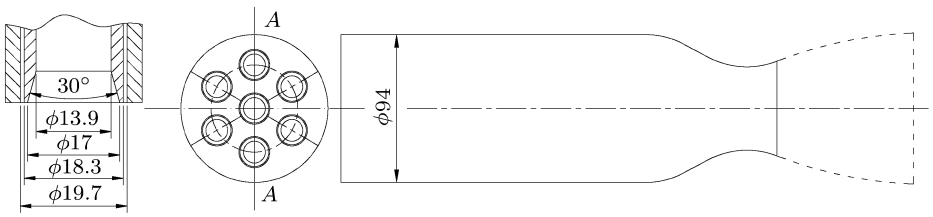


Fig. 1. Prototype shear-coaxial element and chamber.

4.1. Numerical models

Great effort has been made to perform CFD simulation of gas–gas combustion flow at Pennsylvania State University (PSU), NASA MSFC (Marshall Space Flight Center), the University of Michigan, *et al.*[7−9,11,16,18] The results indicated that the steady Reynolds–Average Navier–Stokes (RANS) method combined with a $k-\varepsilon$ turbulence model did not have the same high-fidelity as the unsteady Reynolds–Average Navier–Stokes (URANS) and the Large Eddy Simulation (LES) techniques in obtaining transient solutions, while the RANS method could effectively simulate the whole combustion flow and obtain statistical average solutions that can match the experimental results. In this study, the RANS method

combined with a $k-\varepsilon$ turbulence model was used to compare different conditions in statistical states instead of being used to accurately investigate transient flowfield solutions. It has turned out to be a feasible approach.

Obtained by using the chemical dynamics model of gaseous hydrogen and gaseous oxygen as shown in Ref. [26], the results of the Eddy–Dissipation Model with a single-step reaction and a 6-species/9-step reaction model (where the chemical reaction was modelled with an Arrhenius formulation) were compared with the experimental results. The whole flowfield structures obtained by these two models are almost the same, which accords well with the experimental result. This conclusion also verifies that the chemical reaction dynamics has little influence on the whole flowfield. In contrast with a multi-species/multi-step model, the combustion temperature is too high to be practicable for the Eddy–Dissipation Model. Since there is just a subtle difference in the result between the 6-species/9-step reaction model and the other multi-species/multi-step reaction model as shown in Ref. [18], the former one is adopted in this paper.

The constant pressure specific heat of each species was calculated as a function of temperature

$$C/R = a_0 + a_1 T + a_2 T^2 + a_3 T^3 + a_4 T^4 + a_5 T^5. \quad (7)$$

In the momentum equations, the transport coefficient $\mu_{\text{eff}} = \mu + \mu_t$, where μ_t is the coefficient of eddy viscosity, and $\mu_t = \rho C_\mu k^2/\varepsilon$. Coefficients of laminar viscosity and heat conduction of a single component were calculated by molecular dynamics. The compressibility of the gas propellants at high pressure was considered. The $R-K$ equation was substituted for the ideal state equation to take the real gas effect into account.

4.2. Numerical method and boundary condition

The entire system was solved by a strongly coupled implicit time-marching method using ADI factorization for the inversion of the implicit operator. Convective terms were 2-order flux split upwind differenced, whereas diffusion terms were centrally differenced.

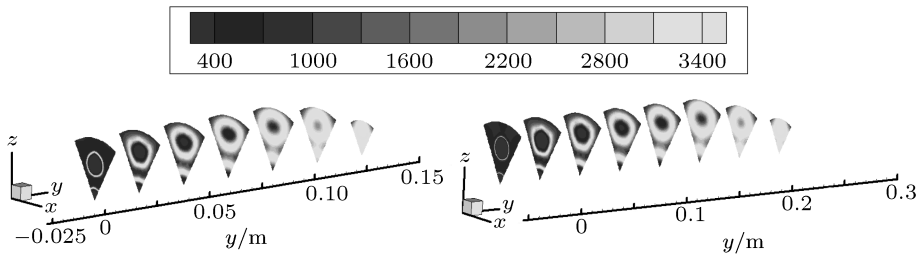
As a result of the non-axisymmetric nature of the injector element, a 60° pie section of the chamber, encompassing a complete element, was modelled. Radial and axial stretchings of the grid were used near the wall boundary and in the shear layer domain. The grid of the symmetric boundary in the cylinder was 44×200. The inlets had a fixed mass flowrate, and the inlet turbulence intensities were both set to be 5%. The nozzle exit was specified as a supersonic outlet. Adiabatic non-slip wall boundaries were used on the chamber walls. Two symmetric sides of the model were set as symmetric boundaries.

4.3. Geometric scaling

In the calculation of geometric scaling, the nominal chamber pressures were kept at 3.0 MPa. The model was designed by reducing all lengths of the prototype by a universal linear scale factor of 2.0. The mass flowrates of propellants should be reduced to 1/4 that of the prototype to keep their injection velocities constant. The parameters are shown in Table 2, indicating that the conditions of the scaling criterion are satisfied. The values of R_{e} for the oxygen jets in the three conditions were $4\times10^5-8\times10^5$, and those for the hydrogen jets were $1.13\times10^5-2.26\times10^5$. The flows were treated as in the turbulent states. The solutions were solved to achieve steady state convergences. The results are shown in Figs. 2 and 3.

Table 2. Parameters of model and prototype chambers.

	H_2 flowrate/(g/s)	H_2 temperature/K	H_2 injection velocity/(m/s)	O_2 flowrate/(g/s)	O_2 temperature/K	O_2 injection velocity/(m/s)
prototype	421.4	300	∼ 550	2528.4	300	∼ 60
model	105.35	300	∼ 550	632.1	300	∼ 60



(a) model (b) prototype

Fig. 2. Temperature contours on some sections in two chambers.

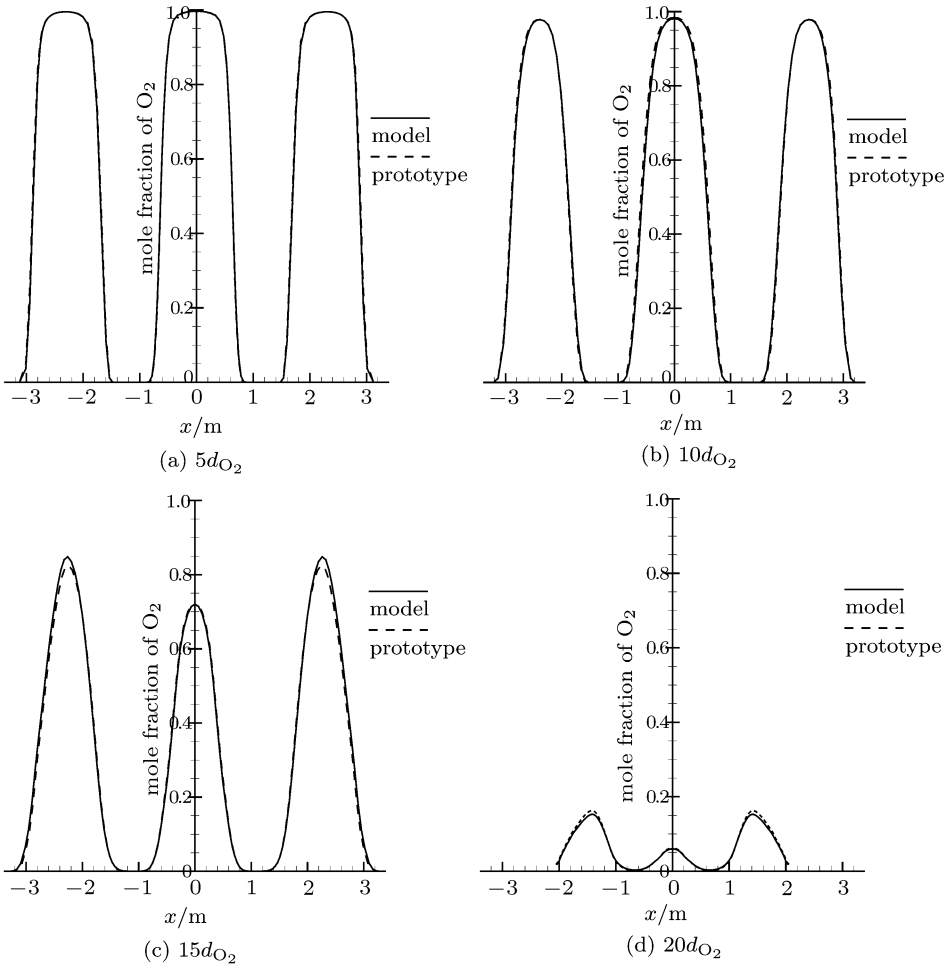


Fig. 3. O_2 mole fraction distributions at the A–A section in two conditions at some typical axial locations.

The temperature contours of the two chambers in Fig. 2 indicate an apparent similarity. Figure 3 shows the O_2 mole fraction distributions at some axial locations in the chambers to quantitatively compare the flow structures. In Fig. 3, the distributions were chosen at the A–A symmetric section shown in Fig. 1, which can represent the characteristics of the flow structure. Because the calculation region contained only half of the A–A section, in Fig. 3 a symmetric treatment was used. To suit the analysis in Section 3 and for convenient comparison, the x-coordinates are set with the ratio of the radial locations to d_{O_2}.

It can be seen from the above that the chamber combustion flowfields are similar both qualitatively and quantitatively. The results numerically validate the theoretical results.

4.4. Pressure scaling

In the calculation of pressure scaling, the dimensions of the chambers were kept unchanged. The prototype chamber studied above was chosen, and the calculation conditions are shown in Table 3, in which three extreme pressures are selected to investigate the greatest distinction and the changing tendency of results. The parameters in Table 3 indicate that the limiting conditions of the scaling criterion are satisfied. The values of Re for the oxygen jets in the three conditions range from 8×10^5 to 5.3×10^6, and those for the hydrogen jets range from 2.26×10^5 to 1.5×10^6. The flows are also treated as in the turbulent states. The results are shown in Figs. 4 and 5 respectively.

The temperature contours of the three conditions in Fig. 4 indicate an apparent similarity. Figure 5 shows the O_2 mole fraction distributions at some axial locations to quantitatively compare the flowfield structures. Figure 5 indicates that three flowfields have almost the same species distributions. When the chamber pressure changes from 3 MPa to 20 MPa, there still exist slight distinctions which are caused by differences in gas compressibility and physical property between different pressure conditions, though the differences are small. The results also numerically validate the theoretical results.

Table 3. Parameters of pressure scaling conditions.

chamber pressure/MPa	H_2 flowrate/(g/s)	H_2 temperature/K	H_2 injection velocity/(m/s)	O_2 flowrate/(g/s)	O_2 temperature/K	O_2 injection velocity/(m/s)
3	0.4214	300	~ 550	2.5284	300	~ 60
10	1.4047	300	~ 550	8.428	300	~ 60
20	2.8094	300	~ 550	16.856	300	~ 60

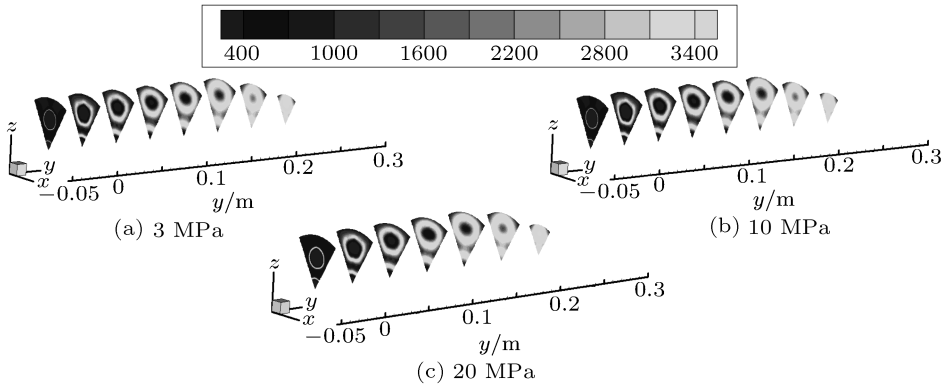
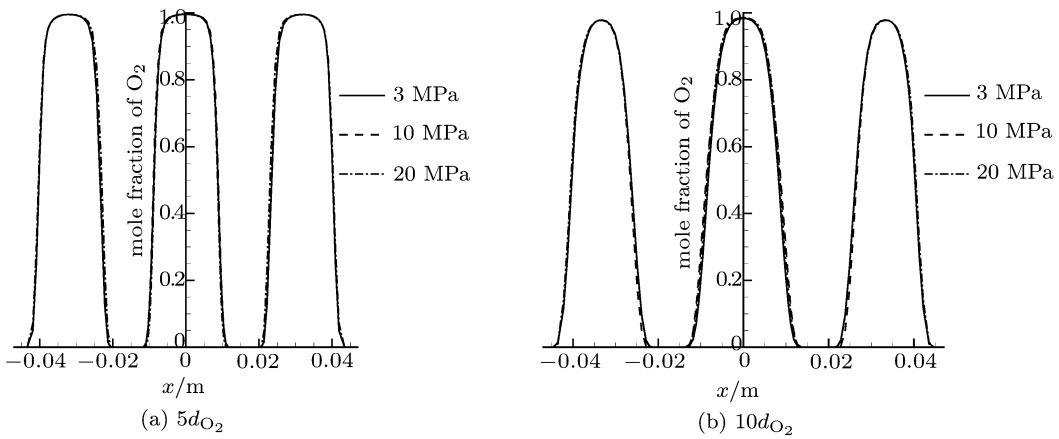


Fig. 4. Temperature contours of the three chamber pressure conditions.



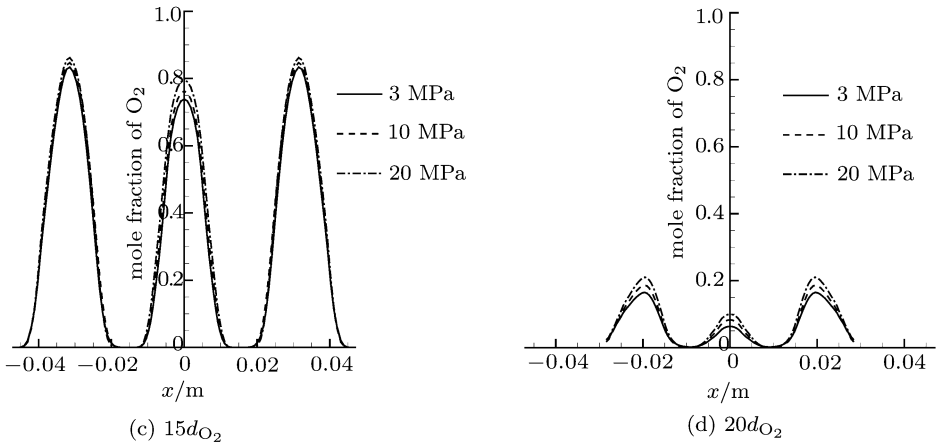


Fig. 5. O_2 mole fraction distributions at the A–A section for three conditions at some typical axial locations.

5. Experimental study

Although numerical simulation conduces to the understanding of the details of flowfield and it can provide prediction and instruction for experiment study, it still cannot substitute for the experiment itself. Up to now no experimental study on the scaling of gas–gas combustion flowfield has been found. However, it was shown in Ref. [13] that in PSU a total of 4 chamber pressure condition tests were carried out, of which two propellant combinations each took place in a single-element chamber, to provide the benchmark combustor wall heat flux data for calculation codes. The ambient-temperature gaseous hydrogen and oxygen, and the products from oxidizer-rich and fuel-rich preburners were used respectively. The chamber pressure ranged from 2.1 MPa to 5.25 MPa. In the tests for each propellant combination, the geometries of the injector/chamber were the same, the propellant temperatures, the injection velocities and the wall boundary conditions were not varied. These conditions totally accord with the scaling ones obtained in this paper. In the tests, the combustor wall temperature and heat flux were measured and the heat flux versus the axial location of the chamber was obtained for each pressure case. The results indicate that the distributions of heat fluxes at different pressures for each propellant combination are quite similar. Since a specific inner flow structure determines a specific heat flux profile and the heat flux profile can reflect a specific inner flow structure, the similar distributions indicate the similarity of the inner flow structures at different pressures. Therefore, it was concluded in Ref. [13] finally that the combustor inner flow structure was independent of the chamber pressure as long as the injector/chamber geometries, the injection temperatures and velocities were kept unchanged.

A similar single-element experimental study with an inner square chamber using gaseous hydrogen and gaseous oxygen was done at the Florida University, USA, and the same conclusions drawn from the study were also described in Ref. [27]. Although the purposes of Refs. [13] and [27] were not to study the scaling or the similarity of gas–gas combustion flow, these single-element experimental studies happen to verify the theoretical conclusion in the present paper. However, the combustion characteristics of a single-element chamber do not involve interaction between the injection elements, which always plays an important role in combustion in a real engine. In this paper an experimental study using a multi-element chamber that can effectively represent a real engine is carried out.

5.1. Experimental facility

A simplified schematic of the system is shown in Fig. 6. The configuration of the multi-element chamber can be seen in Fig. 7. The chamber was modular and could be easily configured to accommodate changes of injector, combustor and nozzle in geometrical configuration. The chamber was designed to serve as a heat sink, the cylinder was of copper, the injector was of stainless steel and the nozzle part was of Wu7Cu. The igniter

was a resonance torch type heated by air. The size and the configuration of the injector and the combustor were designed to be the same as those of the prototype chamber numerically studied in the above section.

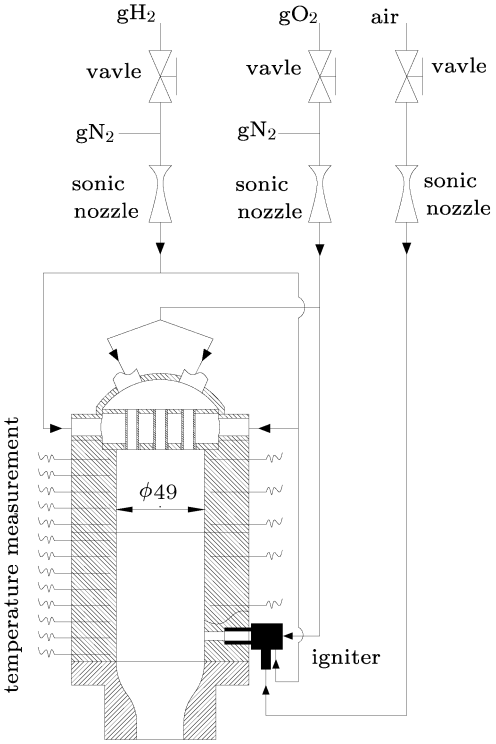


Fig. 6. Facility schematic.

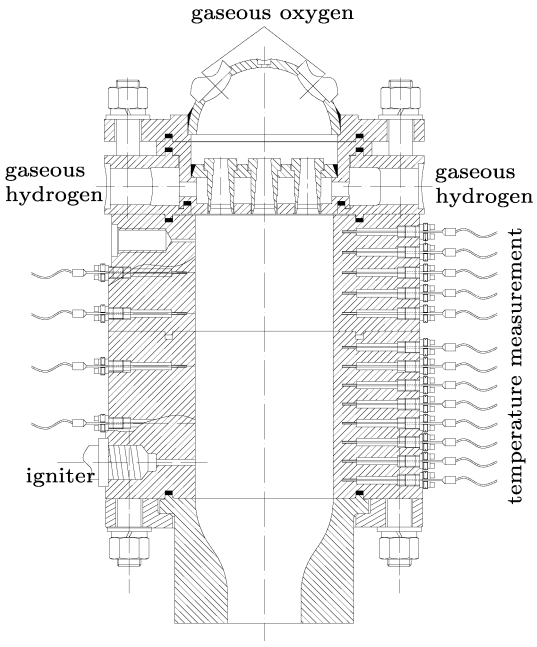


Fig. 7. Schematic of chamber and thermocouple locations.

To examine the similarity in the combustion flowfield structures in different operational conditions, as done in Refs. [13] and [16], the wall temperature measurement method, which was introduced in Ref. [26], was also applied to this study.

5.2. Thermocouple instrumentation and timing

Some small holes with 1.5 mm inner diameter were distributed at the measurement points. The thermocouples were used to measure the temperatures of the bottoms of these holes. Axial locations for instrumentation are indicated in Fig. 7. In the cylinder, the thermocouples were located at some axial intervals. The distances between all the measurement points and the combustor inner wall were the same. Multiple instrumentations (four each) were presented at some axial location, and four thermocouples were separated at 90^0. Figure 8 shows the arrangement of the circumferential locations of the thermocouples.

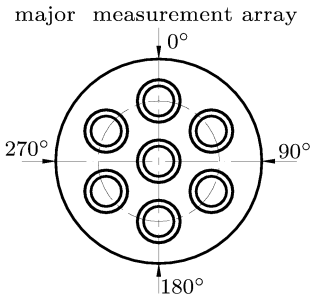


Fig. 8. Arrangement of the thermocouple circumferential locations.

Because of the heat-sink design of the chamber and with the heat protection taken, the tests could be conducted in different durations for different chamber pressure cases: 1.5 MPa-2 s, 2.0 MPa-2 s, 2.5 MPa-2 s, 3.0 MPa-2 s, 3.5 MPa-1.5 s.

5.3. Test conditions

By making full use of the capability of the experimental system, experiments at five pressures and a total flowrate of 3.04 kg/s were carried out. A total of 9 hot-fire tests were conducted steadily. The operational conditions and the typical chamber pressure profiles are summarized in Table 4 and Fig. 9 respectively. The nominal values of MR are 6.0 for all conditions. The parameters shown in Table 4 indicate that all the limiting conditions of the scaling criterion are satisfied.

Table 4. Operational parameters of tests.

chamber pressure/MPa	O_2 flowrate/(g/s)	O_2 temperature/K	O_2 velocity/(m/s)	fuel flowrate/(g/s)	fuel temperature/K	fuel velocity/(m/s)	MR	repeat times
1.64	1111	295	~ 60	186	305	~ 550	5.97	2
2.05	1486	294	~ 60	246	306	~ 550	6.04	2
2.61	1880	295	~ 60	314	308	~ 550	5.99	1
3.02	2170	295	~ 60	368	308	~ 550	5.90	2
3.68	2614	293	~ 60	429	303	~ 550	6.09	2

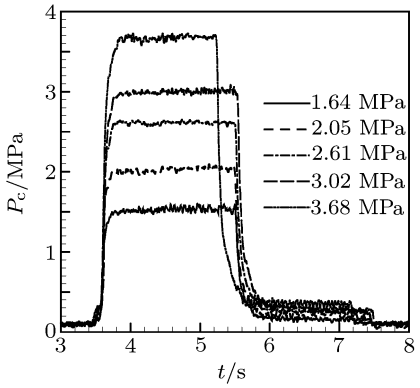


Fig. 9. Typical chamber pressure profiles for five cases.

5.4. Instrumentation behaviour, results and discussion

The time traces of some thermocouples for a representative 2.05 MPa chamber pressure test are shown in Fig. 10. A total of seven sets of thermocouple temperature measurements are also shown in Fig. 10. In terms of nomenclature in the figure, for example, the first trace labelled as TC-40-0° denotes that the thermocouple was at the 40 mm axial location and 0° degrees (the angle was defined with respect to the major array of thermocouples which is shown in Fig. 8). It can be seen that all the temperature traces behave well without noise.

During the steady state portion of the firing, the temperatures went up steadily due to the heat sink nature of the chamber design. The curves of two thermocouples located respectively at 40 mm (at 0° and 180°) and 106 mm (at 90° and 270°) are nearly identical, which suggests that the chamber flowfield was symmetric due to the symmetric injection element layout, thus the thermocouples of the major measurement array can be utilized to evaluate the inner flowfield. According to the heat transfer theory, at the measurement points the greater the heat flux on the inner wall is, the more rapidly the temperature will rise. Therefore, in this paper the heat flux on the inner wall was qualitatively evaluated through the increment of temperatures at the measurement points of the major measurement array during steady firing.

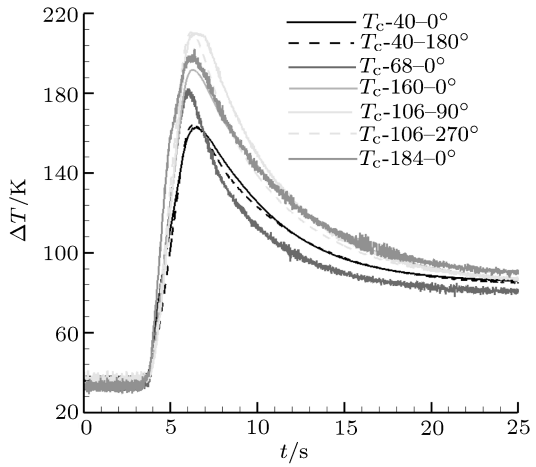


Fig. 10. Thermocouple temperature traces (representative) for a 2.05 MPa test.

The increments of temperature at these measurement points versus the axial distance for the 2.05 MPa chamber pressure case are plotted in Fig. 11, showing that the results of two repetitive tests are nearly identical. The increments of temperatures versus axial distance for all five chamber pressure conditions cases are shown in Fig. 12. The profiles have small peak values near the injector faceplates, and then increase up to their maximum values. The flowfield contours indicate that a recirculation zone exists near the injector face, which causes the first peak value of the wall heat flux. The mixing combustion continues and develops along the axial direction in a region near the measurement points. The high temperature region becomes larger and the axial velocity becomes greater, causing continuous increase of the heat flux on the wall. When the combustion in this region becomes nearly complete, the heat flux reaches the maximum value at some axial point. The slight decline of the

heat flux appearing finally is caused by the decline of maximum heat conduction supporting abilities, because the inner exothermic reactions at this region are almost finished but the heat loss on the wall continues.

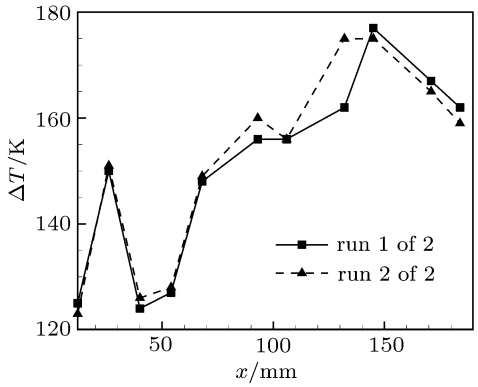


Fig. 11. Curves for wall temperature increment versus axial distance for the 2.05 MPa chamber pressure case.

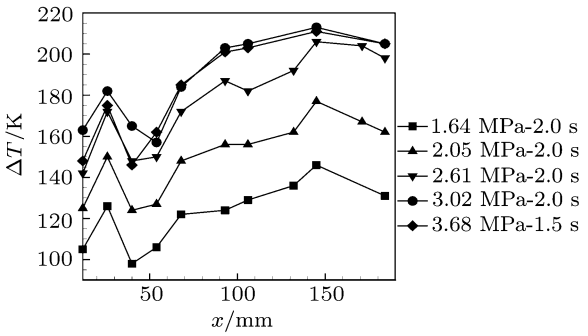


Fig. 12. Curves for wall temperature increment versus axial distance for five chamber pressure cases.

The fact that the distribution trends of all curves are almost identical suggests that the fluid dynamic structures of the five chamber pressure cases are similar. Following the above theoretical conclusion obtained in this paper, which has been experimentally verified in single-element conditions by using the data in Refs. [13] and [27], this experimental result can further verify the theoretical conclusion in a multi-element condition.

In different chamber pressure conditions, when other parameters remain unchanged, the factor that mainly influences the flowfield structure is the difference in compressibility between propellants and products. Table 5 shows the compressibility factors for propellants and main products at different pressures in H_2/O_2 combustors ($Z = p/\rho RT$), with the highest test pressure being 6.21 MPa as in Ref. [27].

Table 5. Values of Z.

T/K	300			≥ 2000		
p_c/MPa	1.64	6.21	20	1.64	6.21	20
H_2	1.01	1.038	1.062	~ 1.0	~ 1.0	~ 1.0
O_2	0.99	0.961	0.946	~ 1.0	~ 1.0	~ 1.0
OH	–	–	–	~ 1.0	~ 1.0	~ 1.0
H_2O	–	–	–	~ 1.0	~ 1.0	~ 1.0

In Table 5, it can be seen that the combustor pressure mainly influences the compressibilities of H_2 and O_2. Even at ambient temperature, the Z values of H_2 and O_2 change by about 2.8% and 2.9% respectively from 1.64 MPa to 6.21 MPa, and about 2.3% and 1.6% respectively from 6.1 MPa to 20 MPa. The change is very small. Furthermore, Figs. 3 and 5 show that temperature of the flowfield in the combustor is very high except in partial domains near the injector face. Gases at high temperature can be considered as ideal ones and the compressibility factors become 1.0. Therefore, when the chamber pressure changes from 6.21 MPa to 20 MPa, the inner flow structures will still be similar as long as the scaling criterion is satisfied.

6. Conclusions

A scaling criterion of the gas–gas combustion flowfield is obtained by conducting a formulation analysis of the gaseous multi-component mixing combustion 3D Navier–Stokes equations and a dimensional analysis of the gas–gas combustion phenomenon. Numerical and experimental studies of multi-element gas–gas injector chambers were carried out to verify the theoretical result. Meanwhile the single-element experimental results in the existing references are utilized. The scaling criterion of the gas–gas combustion flowfield is obtained as follows: a) similarity between the geometries of the injector and the chamber; b) identical propellants; c) constant injection velocities and propellant temperatures; d) non-slip and similar species wall boundary; e) flow in sufficient turbulence conditions. This conclusion is not only suitable for FFSC engines, but also for those engines and combustion devices using gaseous fuels and oxidizers, and the theoretical methods utilized in this paper give a reference for similar studies.

Acknowledgment

The authors thank Beijing Space Propulsion Experiment Center for the experimental facilities. They also thank Zhu N C from Institute No. 11 of the Ministry of Aerospace Industry, and Zhang W and Li Sh from Beijing West Zhonghang Technology Ltd. for help in designing the thermocouples. Finally, the authors thank all the people who made contributions and gave much help to this paper.

References

[1] Penner S S 1955 *Combustion Research and Review*, AGARD Combustion Colloquium (London: Butterworths) p140

[2] Penner S S 1957 *Chemical Problems in Jet Propulsion* (London: Pergamon) p345-347, p376-388

[3] Dexter C E, Fisher M F, Hulka J R, Denisov K P, Shibanov A A and Agarkov A F 2004 *Liquid Rocket Thrust Chambers: Aspects of Modeling, Analysis, and Design*, edited by Yang V, Habiballah M, Hulka J and Popp M *Progress in Astronautics and Aeronautics* **200** p553

[4] Kenny R J, Moser M D, Hulka J R and Jones G 2006 *AIAA* Paper 2006–4705

[5] Hulka J R 2008 *AIAA* Paper 2008–5113

[6] Davis J A and Campbell R L 1997 *AIAA* Paper 1997–3318

[7] Foust M J, Deshpande M, Pal S, Ni T, Merkle C L and Santoro R J 1996 *AIAA* Paper 1996–0646

[8] Schley C A, Hagemann G and Tucker P K 1997 *AIAA* Paper 1997–3302

[9] Tucker P K, Klemt M D and Smith T D 1997 *AIAA* Paper 1997–3350

[10] Farhangi S, Yu T, Rojas L, Sprouse K and McKinnon J 1999 *AIAA* Paper 1999–2757

[11] Archambault M R, Talley D and Peroomian O 2002 *AIAA* Paper 2002–1088

[12] Smith T D, Klem M D and Breisacher K J 2002 NASA/TM-2002-211982

[13] Marshall W M, Pal S, Woodward R D and Santoro R J 2005 *AIAA* Paper 2005–3572

[14] Lin J, West J S, Williamst R W, Tucker P K and Chenoweth J D 2005 *AIAA* Paper 2005–4524

[15] Tucker P K, Menon S, Merkle C L, Oefelein J C and Yang V 2007 *AIAA* Paper 2007–5572

[16] Tucker P K, Menon S, Merkle C L, Oefelein J C and Yang V 2008 *AIAA* Paper 2008–5226

[17] Vaidyanathan R, Tucker P K, Papial N and Shyy W 2004 *J. Propul Power* **20** 705

[18] Sozer E, Vaidyanathan A, Segal C and Shyy W 2009 *AIAA* Paper 2009–449

[19] Calhoon D, Ito J and Kors D 1973 NASA CR-121234, Contract NAS3-13379

[20] Wim A. de Groot, Thomas J. McGuire and Steven J. Schneider 1997 *AIAA* Paper No.1997–2847

[21] Zhou L X 1993 *Theory and Numerical Modeling of Turbulent Has-Particle Flows and Combustion* (Beijing: Science Press and CRC Press)

[22] Gao Y W 2002 *Experimental Fluid Dynamics* (Xian: China Northwestern Polytechnical University Press)

[23] Bian B M, He A Z, Li Z H, Yang L, Zhang P, Shen Z H and Ni X W 2005 *Acta Phys. Sin.* **54** 5534 (in Chinese)

[24] Anderson W E, Ryan H M, Santoro R J and Hewitt R A 1995 *AIAA* Paper No. 1995–2357

[25] Hewitt R A 2006 *Combustion Instability in Liquid Rockets* (with a d/V Correlation Perspective), invited lecture delivered at the 31st AIAA/ASME/SAE/ASEE Joint Propulsion Conference

[26] Wang X W, Jin P and Cai G B 2009 *Journal of Beijing University of Aeronautics and Astronautics* 35 (in Chinese)

[27] Alex C, Aravind V and Corin S 2007 *J. Spacecraft Rockets* **44** 633